PERGAMON

Corrosion Science 43 (2001) 1019–1030

CORROSION SCIENCE

www.elsevier.com/locate/corsci

Potentiodynamic tests and electrochemical impedance spectroscopy of injection molded 316L steel in NaCl solution

Ana V.C. Sobral [a], W. Ristow Jr. [b], Denise S. Azambuja [c], Isolda Costa [d], César V. Franco [a,*]

[a] *LEC/LABMAT, Depto. de Química-CFM, Universidade Federal de Santa Catarina, Campus Trindade-UFSC, 88040-900 Florianópolis SC, Brazil*

[b] *LUPATECH S/A Divisão STEELINJECT Caixa, Postal 1215, Distrito Industrial, 95112-090 Caxias do Sul RS, Brazil*

[c] *Instituto de Química, UFRGS, 91501-970 Porto Alegre RS, Brazil*

[d] *Departamento de Engenharia e Ciência dos Materiais, Instituto de Pesquisas Energéticas Nucleares – IPEN/CNEN-SP, Caixa Postal 11049, 05422-970 São Paulo SP, Brazil*

Received 8 September 1999; accepted 17 July 2000

Abstract

Cyclic polarization tests of injection molded 316L steel were carried out in 3% NaCl solution. The microstructure of the as-tested samples was studied by optical and scanning electron microscopy. The corrosion resistance of injection molded 316L steel was also evaluated studying the evolution of electrochemical impedance spectroscopy at the open-circuit potential for immersion periods varying from 1 to 78 days in aerated salt solution. The penetration of the electrolyte solution through surface open pores as a function of the immersion time has also been addressed so the effect of porosity on the corrosion behavior was investigated. The results demonstrated that the corrosion resistance of the injected steel is affected by the presence of open pores, as they act towards increasing the effective surface area of the material. This fact was confirmed by an increase in the corresponding value of the double layer capacitance, C_{dc}, and a decrease in the value of the charge transfer resistance, R_t.

Keywords: Corrosion; Injection molding; Sintered steel; Electrochemical impedance spectroscopy

* Corresponding author. Tel.: +55-48-331-9765; fax: +55-48-331-9711.
E-mail address: franco@materiais.ufsc.br (C.V. Franco).

0010-938X/01/$ - see front matter
PII: S0010-938X(00)00140-2

1. Introduction

Several recent investigations have demonstrated a particular interest in the corrosion behavior of sintered steels with different alloying elements and porosity [1–7]. The corrosion resistance of sintered materials is considerably reduced by inherently residual open porosity. Excessive open porosity may expose the core material to corrosive environments by increasing surface area. Consequently, crevice corrosion may take place [7] with the formation of concentration cells within the pores, reducing the passivity of the sintered alloy [8,9]. Further confirmation to this fact has been provided by Otero et al. [10] for 316L and 304L steels in organic acids.

Injection molding has been applied to powdered materials as an alternative route to manufacture corrosion-resistant sintered components. This process has been proved excellent in the production of structural parts, as its characteristics include design flexibility and low cost. Consequently, the interest in this technique has increased over the past 20 years. The fundamental principles of this technique are closely related to microfusion, and it represents a significant technological breakthrough in powder metallurgy. Injection molded alloys generally include few and rounded pores, connected by narrow channels through the material. Fine powders (<25 μm) are commonly used resulting in sintered densities of about 98% of the theoretical density of the alloy. These microstructural features improve the corrosion behavior of the material exposed to a chemically hostile environment. Among several applications, powder injection molded (PIM) materials may be especially important in orthodontic components and surgical instruments. In particular, 316L steel can be injection molded to yield cost-efficient parts.

In this study, the corrosion characteristics of PIM 316L steel in NaCl 3% solution were investigated by electrochemical impedance spectroscopy (EIS) and cyclic polarization tests. EIS analyses allowed to follow the evolution of the open-circuit impedance as a function of immersion time. Although similar studies have been carried out on cast austenitic 316L steel [11], the present investigation represents the foremost EIS study published on sintered injection molded steel.

2. Experimental methods

2.1. Injection molding outline

The injection molding procedure can be divided into four stages: (a) raw-material preparation, (b) injection molding, (c) dewaxing and (d) sintering [12]. To assure optimum performance of the injected material, the starting powders were mixed with organic components containing a mixture of thermoplastics, wax, oils, lubricants and surfactants, altogether referred as ligand. The raw material was chosen to optimize the formation of a continuous film in the surface of each powder particle, upon mixing. Additionally, the ligand must not be aggressive to the particle surface and should be thermally stable. An important point to be emphasized during the injection molding procedure is the design of the mold cavity, which must allow a

Table 1
Composition of injection molded 316L steel used in this study

Element	C	Si	Mn	P	S	Ni	Cr	Mo	Cu
(wt.%)	0.013	0.80	0.20	0.031	0.003	13.5	16.40	2.2	–

progressive and even distribution of the powder mixture to prevent the separation of the powder from the ligand, and to keep the powder density and sedimentation gradients at acceptable levels. The duration of an injection procedure depends on the cavity geometry, viscosity of the mixture, and injection pressure. After the injection procedure is completed, the injected material must be cooled to increase hardness and resistance. Dewaxing consists in extracting the ligand and is performed both by chemical dissolution and thermal degradation. In the chemical extraction, the low melting point and volatile components of the ligand are dissolved, reducing the content of ligand in the injected part and opening channels for the thermal degradation stage. During this step, residual ligand is removed by evaporation mechanisms and capillary flow in liquid state. The application of both techniques allows efficient ligand extraction. Finally, sintering is accomplished under vacuum using a controlled atmosphere furnace. The 316L PIM samples used in this investigation were supplied by LUPATECH, Steelinject, Caxias do Sul, Brazil. Pre-sintering was performed at 980°C for 1 h under H_2 atmosphere. Sintering was carried out at 1300°C for 4 h in a reducing (vacuum) atmosphere of argon/hydrogen. The final density of the sintered material was 7.59 $g\,cm^{-3}$. Assuming a theoretical density of 8 $g\,cm^{-3}$, porosity was estimated at 4%. Table 1 displays the chemical composition of the 316L steel used in this study.

2.2. Surface preparation

The working electrodes were surfaces prepared using emery papers from 220 to 600 mesh in water suspension. Next, the surfaces were polished in alumina slurry (0.25 μm) to a mirror finish. Finally, the electrodes were, rinsed in water and alcohol and dried prior to immersion in NaCl solution. The dewaxing were performed by the use of organic solvents.

2.3. Electrochemical tests

Cyclic potentiodynamic tests were carried out in a three electrode system in a quiescent non-deaerated electrolyte, which was chosen to simulate real conditions. However, it has been established that the presence of oxygen in the electrolyte might raise the open-circuit corrosion potential above the pitting and repassivation potentials, and austenitic stainless steels may pit in aerated dilute salt solutions. A Princeton Applied Research Galvanostat/Potentiostat model 283 was used. For this series of tests, the samples were scanned from −250 mV vs. OCP up to the point where a significant current increase was observed in the anodic region. As the scan reached a user-programmed threshold current value and/or an offset potential, it was

reversed and the sample was then scanned in the cathodic (negative) direction. EIS analyses were carried out using EG&G PAR models 273A and 283 potentiostat/galvanostat connected either to a Schlumberger 1255 high frequency analyzer or an EG&G PAR 5210 lock-in amplifier. The scatter in impedance was analyzed by an EG&G PAR 273A electrochemical impedance computer program. The electrochemical cell consisted of three electrodes, i.e, a sample stand to hold the working electrode, a platinum wire auxiliary electrode, and a saturated calomel reference electrode (SCE). The working electrode exposed area was 1 cm^2. A sinusoid a.c. voltage signal of amplitude ± 10 mV was applied in the impedance measurements. The impedance response was determined in the frequency range from 10^5 to 10^{-3} Hz. The open-circuit potential was measured for about 30 min allowing it to reach steady state.

2.4. Microstructural analysis

The microstructure of the samples was assessed by optical microscopy using a LEICA model REICHERT MEF4M system.

2.5. Sensitization evaluation

The susceptibility of the injection molded 316L steel to intergranular attack was evaluated by ASTM A262 standard practice [13]. Specimens of the injection molded 316L steel were tested by Practice A after a sensitizing heat treatment at 675°C for 1 h. Two electrolytic etchings were performed, one in oxalic acid and the other in ammonium persulfate.

3. Results and discussion

The experiments performed in deaerated electrolytes showed similar results to those obtained in aerated electrolytes. All experiments reported in this work were performed in quiescent non-deaerated 3% NaCl electrolytes. Microstructure of injection molded 316L stainless steel – optical microscopy revealed a predominantly austenitic microstructure with corresponding average grain size 41.2 μm. Annealing twins and rounded pores evenly distributed across the steel surface could be observed (Fig. 1). Oxide inclusions were present inside the pores (Fig. 2), confirming the results obtained from other investigations [14,15]. Exposing pore areas with oxides inclusions reduces corrosion resistance. In fact, pit nucleation was noticed from a careful observation of the attacked surface (Fig. 2).

3.1. Sensitization evaluation

In this procedure, two electrolytic etchings were carried out, using oxalic acid and ammonium persulfate. Both produce similar etched structures which corresponded to end-grain pitting I, as shown in Fig. 2. The etched structure of the injection

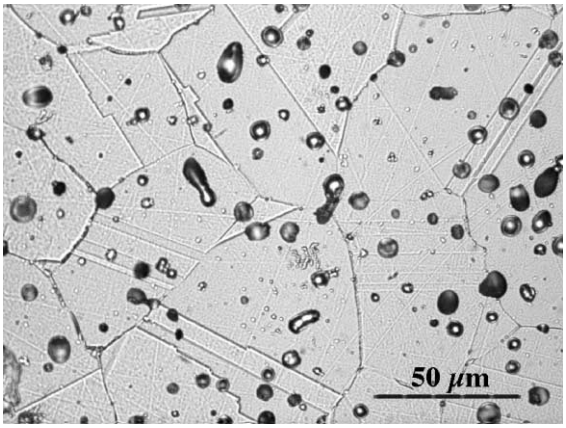

Fig. 1. Optical microscopy of injection molded 316L steel.

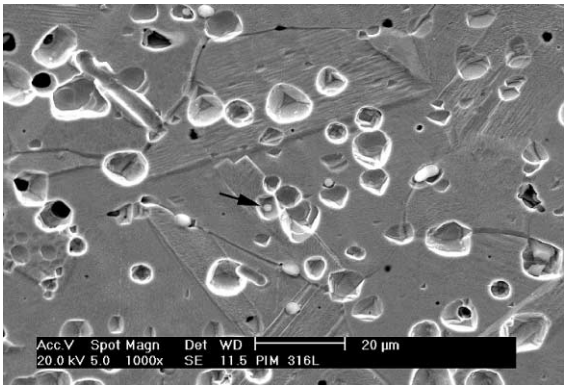

Fig. 2. SEM image of injection molded 316L after electrolytic etching in 10% oxalic acid. Arrow points to SiO_2 particle inside pore.

molded material showed that the steel had no susceptibility to intergranular attack. Rounded particles present inside the pits were observed after electrolytic etching. X-ray dispersive energy spectroscopy revealed that those particles consisted of SiO_2, possibly trapped inside the pores during the manufacturing process, lowering down the pitting resistance of the injection molded steel.

3.2. Open-circuit potential vs. time

Open-circuit potential measurements of injection molded 316L in NaCl 3% displayed a behavior similar to that of chromium, nickel and wrought stainless steel (Fig. 3), with a shift to a nobler region suggesting surface passivation [16].

The surface remained passive in 3% NaCl solution. However, a slight potential oscillation was observed, after a certain potential level, suggesting an aggressive

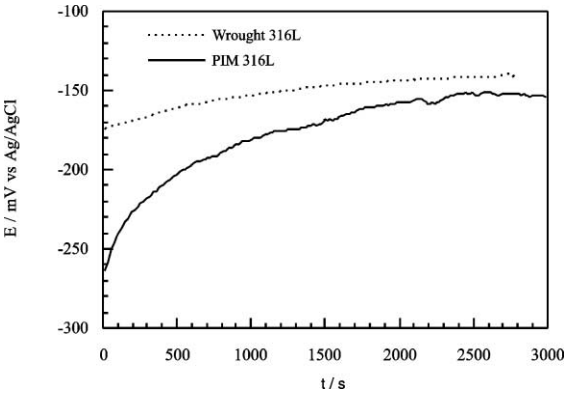

Fig. 3. OCP as a function of time for injection molded 316L steel in NaCl 3% solution.

action of chloride ions towards the passivating layer. In fact, visual inspection of the material revealed that it was highly susceptible to localized corrosion.

3.3. Cyclic potentiodynamic tests

Fig. 4 illustrates the cyclic potentiodynamic behavior of injection molded 316L steel in NaCl 3%. The potential where the loop was closed is referred to as the protection potential E_{prot} [17]. Pits grow between E_{prot} and E_{pit}, but the nucleation of new pits only takes place above E_{pit}. Below E_{prot} pit growth is not observed. Usually, E_{prot} and E_{pit} are determined in deaerated solutions to avoid the open-circuit potential to raise above the pitting and repassivation potentials. The values of E_{prot} and E_{corr} on Fig. 4 are rather similar, which indicates that pitting occurs at the open-circuit potential in the aerated salt solution.

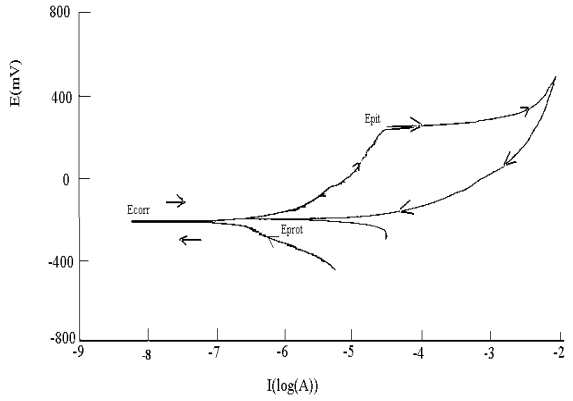

Fig. 4. Cyclic polarization of injection molded 316L in NaCl 3%. Scan rate of 0.8 $mV\,s^{-1}$, threshold current 0.2 $mA\,cm^{-2}$, onset potential −250 mV vs. (OCP).

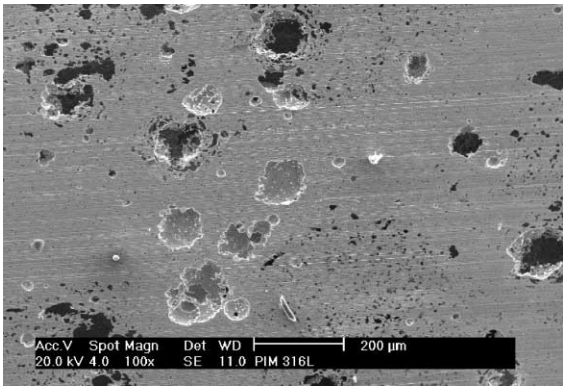

Fig. 5. SEM image of PIM 316L after cyclic polarization in NaCl 3%, illustrating pitting.

The current density observed in the initial scan was two orders of magnitude lower than that of the reversed scan. The anodic polarization revealed the presence of an unstable passivation region between −200 and 200 mV vs. SCE, followed by a significant increase in the current density at the region corresponding to pit growth ($E = 200$ mV vs SCE).

It has been reported [18,19] that E_{pit} usually lies within the range of 200 and 270 mV vs. SCE for conventional 316L steel, which is in good agreement with the value found for the injection molded steel. E_{prot} values were all around −200 mV vs. SCE. Fig. 5 illustrates the surface of a sample subjected to a cyclic potentiodynamic polarization scan in NaCl 3% solution. Initially, a threshold current of 0.2 mA cm^{-2} was reached. The scan was then reversed to its initial open-circuit potential. Pits were formed on various regions of the injection molded 316L surface. Shallow and deep pits corresponding to unstable and stable pits, respectively, were seen on the PIM 316L steel after cyclic polarization. The bottom of the unstable pits must have passivated after the initiation period whereas favorable conditions for the growth of stable pits were met. Fig. 6 shows a general view of one of the pits formed, displaying the external surface surrounding the pit (Fig. 6a) and the surface at the bottom of the pit (Fig. 6b). It can be seen that, at the bottom of the pit, round silica particles were found. It was previously suggested that the presence of such particles inside the pores might have led to pit initiation. Fig. 6b suggests that they might have also been responsible for the growth of stable pits. The pit morphology was irregular, similarly to that found for pits on conventional stainless steels (Fig. 7).

3.4. Electrochemical impedance spectroscopy

Impedance diagrams were obtained for different immersion periods in NaCl 3% solution: 1, 7, 14, 16, 31, and 78 days. Fig. 8 shows the presence of a single capacitive arc obtained from the sample immersed for 7 days, which implies in a time relaxation constant [20].

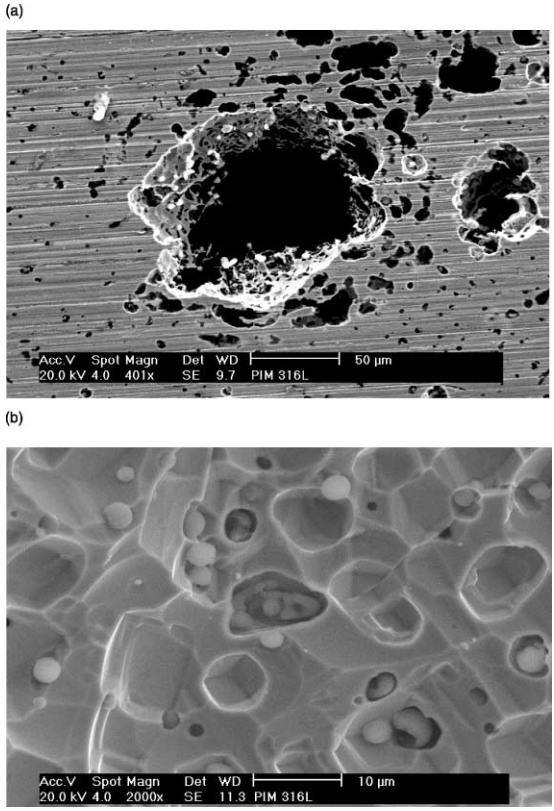

Fig. 6. Pit formed after cyclic polarization of PIM 316L in NaCl 3%: (a) general view of the pit and (b) surface at the pit bottom.

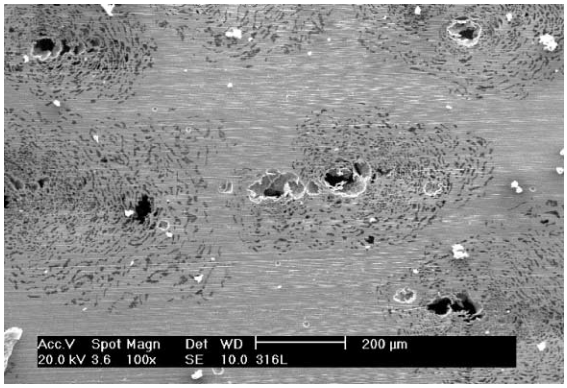

Fig. 7. SEM image of the surface of conventional 316L steel after cyclic polarization in NaCl 3%.

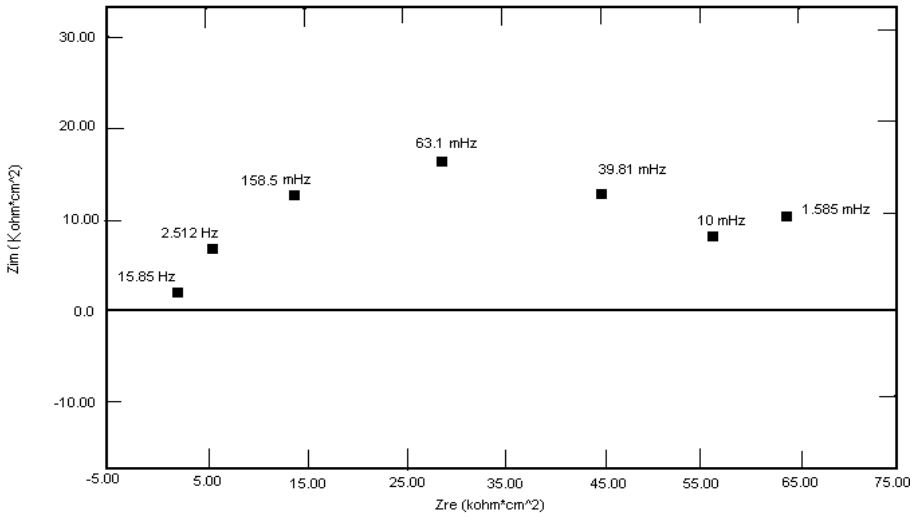

Fig. 8. Impedance plot after 7 days in NaCl 3%.

The semicircle is flattened and offset from its real axis, departing from the behavior typically observed for a simple RC circuit [21]. The porous nature of the injection molded material may explain those variations, on the basis of the distribution of the resistive and capacitive elements in the electrode [22]. The solution resistance, R_s, can be obtained extrapolating the impedance values to higher frequencies. Moreover, the diameter of the semicircle corresponds to the resistance to charge transfer, R_t, whereas its intersection at low frequencies to $R_s + R_t$. The double layer capacitance, C_{dl}, can be calculated from

$$C_{dl} = 1/2\pi f_{max} R_t \tag{1}$$

resulting in 19.6 $\mu F\,cm^{-2}$ for 316L injection molded steel. The value of R_t estimated was 51 $k\Omega\,cm^2$.

Samples immersed for 14 days featured further flattening of the semicircle, which could be attributed to a corresponding increase of the effective surface in contact with the electrolyte. This increase in the effective surface might also have caused a corrosion potential shift to more negative values. Consequently, a decrease in R_t to 3.2 $k\Omega\,cm^2$ and increase in C_{dl} to 31.6 $\mu F\,cm^{-2}$ were observed. The impedance plot of samples immersed for 16 days (Fig. 9) displayed two capacitive arcs, one at the low frequency and another at the high-frequency region. R_t decreased to 18 $\Omega\,cm^2$, and the overall behavior indicated a general reduction of the corrosion resistance at this immersion period [19,20].

The relatively high value of C_{dl} obtained could be attributed to an association of effects including the non-homogenous aspect of the surface [20], the presence of pores [23], and the adsorption of intermediate compounds [24]. Table 2 summarizes

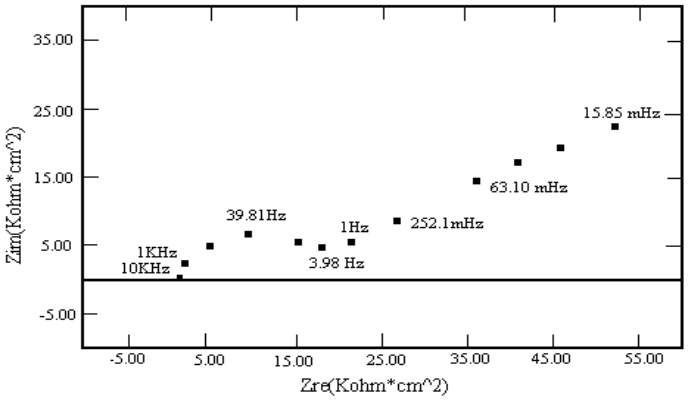

Fig. 9. Impedance plot after 16 days in NaCl 3%.

Table 2
Electrochemical impedance data as a function of immersion time

Time (days)	R_t ($k\Omega\,cm^{-2}$)	C_{dc} ($\mu F\,cm^{-2}$)	E_{corr} (V vs. SCE)
7	51	19.6	−0.22
14	3.2	31.6	−0.40
16	18×10^{-3}	200	−0.49
31	15×10^{-3}	230	−0.52
78	12×10^{-3}	250	−0.58

the results acquired from impedance plots corresponding to different immersion periods.

It can be noticed that E_{corr} shifted to lower values as the immersion time increased. Concurrently, R_t decreased and C_{dl} increased. However such variations were only abrupt during the first 16 days of immersion, when a single capacitive arc was observed. As soon as the second arc was formed (Fig. 9), the variations of E_{corr}, R_t, and C_{dl} became less significant. The contour of the impedance plots (not shown) obtained after 78 days resemble that of Fig. 9, and is a result of the combined action of merely resistive and capacitive elements.

The kinetics of the corrosion process can be evaluated from the impedance plots, as suggested by Park and Macdonald [25]. For that, $\log 1/(Z_{\omega\to 0} - Z_{\omega\to\infty})$ should be plotted as a function of the immersion time. $Z_{\omega\to 0}$ represents the polarization resistance, including the resistance to both charge and mass transport across the substrate and the corrosion product film. This parameter is, in turn, inversely proportional to the instantaneous corrosion rate given by Stern–Geary's equation [26]. Data gathered herein indicated that up to 14 days, 316L steel is subjected to a linear corrosion process, whose rate subsequently increases in the following couple of days. This is probably a consequence of an increase in the contact area between substrate and electrolyte, due to the presence of pores and the decrease in pH within the pores. Beyond 16 days, the corrosion rate stabilized due to film thickening, which

blocked the pores and inhibit the diffusion of chloride ions. No significant changes could be observed after 31 days of immersion. However, R_t decreased and E_{corr} shifted to lower values. The observed Warburg impedance may be due to (i) diffusion through the porous stainless steel substrate, (ii) a porous corrosion-product surface film, or (iii) the near-surface deaerated electrolyte layer formed under concentration-polarization control during corrosion in an aerated electrolyte.

4. Conclusions

The results indicated that injection molded 316L steel is mainly subjected to pitting corrosion. Microstructural analysis revealed a relationship between porosity, the presence of oxide inclusions inside the pores and the formation of pits. Injection molded 316L steel did not show any susceptibility to intergranular corrosion. Although the double layer capacitance, C_{dl}, increased and the charge transfer resistance, R_t, decreased with immersion time, the corrosion rate stabilized after a certain period of time. It has been proposed that the porosity, and consequently, the effective area of the electrode exposed to the electrolyte solution, increased with immersion time, and this was responsible for the increase in C_{dl}. Further work regarding pit characterization is currently under way.

Acknowledgements

PRONEX, CNPq and CAPES.

References

[1] P.C. Borges, N.C. Pereira, C.V. Franco, A.N. Klein, Adv. Powder Metall. Particul. Mater. 2 (1994) 61.
[2] A.V.C. Sobral, A.M. Maliska, G. Tosi, J.L.R. Muzart, A.N. Klein, C.V. Franco, Adv. Powder Metall. Particul. Mater. 3 (11) (1995) 57.
[3] N.C. Pereira, F.G. Mittelstadt, A. Spinelli, C.V. Franco, A.M. Maliska, A.N. Klein, J.L.R. Muzart, J. Mater. Sci. 30 (1995) 4817.
[4] A.V.C. Sobral, Caracterização Eletroquímica e Metalográfica de Aços Sinterizados e Nitretados, Master Thesis, Depto. de Química, Universidade Federal de Santa Catarina, SC, Brazil, 1996.
[5] A.V.C. Sobral, A.C. Boblitz Parente, J.L.R. Muzart, C.V. Franco, Surf. Coat. Technol. 92 (1997) 10.
[6] E. Maahn, S.K. Jensen, R.M. Larsen, T. Mathiesen, Adv. Powder Metall. Particul. Mater. 7 (1994) 253.
[7] T. Mathiesen, E. Maahn, Adv. Powder Metall. Particul. Mater. 3 (1995) 45.
[8] L. Fedrizzi, F. Deflorian, A. Tiziani, I. Cristofolini, A. Molinari, Adv. Powder Metall. Particul. Mater. 7 (1994) 273.
[9] A. Tremblay, R. Angers, Adv. Powder Metall. Particul. Mater. 7 (1995) 225.
[10] E. Otero, A. Pardo, M.V. Utrilla, F.J. Pérez, C. Merino, Corros. Sci. 39 (1997) 453.
[11] J.L. Dawson, M.G. Ferreira, Corros. Sci. 26 (1986) 1009.

[12] R.M. German, Powder Injection Molding, second ed. Metal Powder Industries Federation, Princeton, New Jersey, 1994.
[13] ASTM Standard Practice A262, Practices for Detecting Susceptibility to Intergranular Attack in Austenitic Stainless Steels, Practice A, Annual Book of ASTM Standards, vol. 3.02, 1988, p. 4.
[14] A.V.C. Sobral, A.C.B. Parente, A.N. Klein, J.L.R. Muzart, C.V. Franco, Adv. Powder Metall. Particul. Mater. 13 (1996) 167.
[15] M.K. Bulger, A.R. Erickson, Adv. Powder Metall. Particul. Mater. 4 (1994) 197.
[16] H.S. Isaacs, Corros. Sci. 29 (1989) 313.
[17] J.A. Dennys, Principles and Preventation of Corrosion, Macmillan, New York, 1991.
[18] A. Sedriks, Corrosion of Stainless Steels, Wiley, New York, 1979.
[19] J.N. Murry, P.J. Moran, E. Gileadi, Corrosion 44 (1988) 533.
[20] D.C. Silverman, J.E. Carrico, Corrosion 44 (1988) 280.
[21] J. Walaszkowski, J. Orllikowski, R. Juchniewicz, Corros. Sci. 37 (1995) 1143.
[22] G.W. Walter, Corros. Sci. 26 (1986) 681.
[23] D.D. Macdonald, H. Song, K. Makela, K. Yoshida, Corrosion 49 (1993) 8.
[24] J.O'M. Bockris, A.K.N Reddy, Modern Electrochemistry, vol. 2, Plenum Press, New York, 1976 (Chapter 11).
[25] J.R. Park, D.D. Macdonald, Corros. Sci. 23 (1983) 295.
[26] M. Stern, A.L. Geary, J. Electrochem. Soc. 104 (1957) 56.